Available online at www.sciencedirect.com

ScienceDirect

Procedia Structural Integrity 35 (2022) 219–227

Structural Integrity Procedia

www.elsevier.com/locate/procedia

2nd International Workshop on Plasticity, Damage and Fracture of Engineering Materials

Crystal plasticity modeling of additively manufactured metallic microstructures

Sadik Sefa Acar[a,b], Orhun Bulut[a], Tuncay Yalçinkaya[a,*]

[a] *Department of Aerospace Engineering, Middle East Technical Universty, Ankara 06800, Turkey*
[b] *Repkon Machine and Tool Industry and Trade Inc., Istanbul 34980, Turkey*

Abstract

Different manufacturing processes such as flow forming, rolling, wire drawing and additive manufacturing induce anisotropic grain structure and texture evolution at the micro scale, which results in macroscopic anisotropic plastic behavior. Among these microstructures, development of columnar grain structure is quite common especially in additively manufactured metallic materials. A systematic micromechanical analysis is necessary to evaluate the influence of both grain morphology and texture (orientation alignment) on the mechanical response of the metallic alloys produced through such innovative techniques. In this context, the objective of the present study is to investigate qualitatively the influence of the columnar grain morphology and the orientation alignment observed in additively manufactured alloys through crystal plasticity finite element (CPFEM) simulations in representative volume elements (RVEs). Different RVEs are generated through Voronoi tessellation and subjected to uniaxial tensile loading in different directions. A detailed analysis is conducted to evaluate the influence of grain structure and orientation alignment on the plastic behavior of the material through homogenization for different microstructures.

Keywords: Crystal plasticity; Additive manufacturing; Anisotropic microstructure; Texture

1. Introduction

Understanding the microstructure and crystallographic texture evolution during manufacturing processes is essential since the mechanical behavior of the final product is strongly dependent on the grain size, shape and texture. Having oriented grains in certain direction results in an anisotropic, direction-sensitive response (see e.g. Zhao et al. (2021)). To achieve the required mechanical properties, ground knowledge on how forming processes affect the crystallographic structure is required. During manufacturing processes such as flow forming, sheet rolling, extrusion and additive manufacturing, crystallographic structure plays a key role since it determines material flow during the process as well as the plastic anisotropy of the final product (see e.g. Zhou et al. (2015), Karakaş et al. (2021)). In industrial

* Corresponding author. Tel.: +903122104258 ; fax: +903122104250.
E-mail address: yalcinka@metu.edu.tr

2452-3216
10.1016/j.prostr.2021.12.068

applications of forming processes, especially in additive manufacturing, grains are observed to be in a shape that deviated from equiaxed morphology (see e.g. Yasa et al. (2011), Qiu et al. (2013), Song et al. (2015)). In addition to that, additively manufactured products contain porous structure (see e.g. Moussaoui et al. (2018); Zhang et al. (2019)). It was established that there is a relation between the evolution of these characteristic morphologies and the mechanical properties. During forming processes, due to thermal and mechanical reasons, grains are appeared to be elongated in certain directions.

Anisotropic and heterogeneous microstructures as well as preferential crystal orientations are observed for additive manufacturing applications such as Powder-Bed Fusion (PBF) and Directed Energy Deposition (DED) techniques (see e.g. Kok et al. (2018)). Products of additive manufacturing have grains elongated in the direction along the highest temperature gradient during rapid solidification, resulting in columnar grains (see e.g. Wang et al. (2012), Hovig et al. (2018)). The morphology and the orientation of the additively manufactured microstructures are determined by material properties and process parameters such as scan velocity, laser or beam power, scan strategy and hatch spacing. With the pursuit of optimum mechanical properties, different process parameters have been tested for years. Grain morphologies and crystallographic orientations resulting from the experiments have been analyzed (see e.g. Thijs et al. (2010), Ishimoto et al. (2017), Ishimoto et al. (2021)). Examining the additively manufactured products reveals that emergence of the columnar grain structure is often accompanied by the crystal orientation alignment (see e.g. Charmi et al. (2021)). Moreover, orientations of the grains are related to the proportion of the elongation (i.e. aspect ratio) of grains. In some cases, the grains are so elongated that they started to be called "fibers" whereas, for some other cases, the grain aspect ratio is not that extreme (see e.g. Guden et al. (2021)). Consequently, crystal orientations vary from case to case depending upon the morphology. Corresponding aligned structure results in the plastic anisotropy. In the literature, the combined effect of orientation and morphology resulted in a weaker stress response along the direction in which the crystallographic structure is oriented (see e.g. Lopes et al. (2003); Guden et al. (2021)). In terms of yield and flow stress experiments have shown that materials are weaker in the direction they are textured (see e.g. Dumoulin et al. (2012), Frazier (2014), Zhang et al. (2015)).

Various experimental studies addressed the crystal structure of additively manufactured products. However, it is not possible to conduct a controlled study where the microstructure is designed during the process to examine its influence. Yet it is possible to make such a study using computational techniques. In this context, the current paper addresses this aspect qualitatively by employing micromechanical models. It is essential to assess the effect of the anisotropy step by step, since it may lead to undesired results (see e.g. Frazier (2014)). In the current study, the grain morphology and the crystallographic orientation alignments are evaluated at different levels using crystal plasticity finite element method (see e.g. Yalcinkaya et al. (2008), Yalçinkaya et al. (2021a)). Crystal plasticity studies have focused on the crystal structure of the additively manufactured metallic materials before (see e.g. Dumoulin et al. (2012), Kergaßner et al. (2019), Ghorbanpour et al. (2020)). However, the analysis of the elongation of grains and orientation alignment at different levels have not been done till now. For this purpose the current work concentrates on the modeling of the anisotropic microstructures through representative volume elements (RVEs), having grains with different mean aspect ratios. Starting from the completely randomly oriented equiaxed grains, the effect of the columnar grains which are gradually elongated and oriented along the building direction is evaluated. The material employed is aluminum AA6016 for all simulations to preserve the comparability. Yet, the findings of the study are not exclusive to this material and can be helpful to the assessment of additive manufacturing applications of other metallic materials as well. The porosity of the final products has not been taken into account, yet. The current study presents a preliminary results and it will be detailed with different microstructural details in the near future.

2. Constitutive Modeling

In the current study, a rate dependent finite strain local crystal plasticity model is employed for the analysis of the constructed RVEs. In this classical framework, the deformation gradient $\mathbf{F}$ consists of a plastic part $\mathbf{F}^p$ due to crystallographic slip and an elastic part $\mathbf{F}^e$ due to elastic lattice distortion. Therefore, deformation gradient may be interpreted as multiplication of these parts

$$\mathbf{F} = \mathbf{F}^e \cdot \mathbf{F}^p \tag{1}$$

Current local plasticity method assumes that plastic deformation occurs due to only the crystalline slip. Therefore, only the plastic slip is taken into consideration in plastic deformation. Plastic velocity gradient is obtained according to the below relation where plastic slip rates $\dot{\gamma}$ are integrated over all slip systems where $\mathbf{m}^{\alpha}$ and $\mathbf{n}^{\alpha}$ denote the slip direction and the normal to the slip plane of the slip system α, respectively,

$$\mathbf{L}_p = \mathbf{D}^p + \mathbf{\Omega}^p = \dot{\mathbf{F}} \cdot (\mathbf{F}^p)^{-1} = \sum_{\alpha=1}^{N} \dot{\gamma}^{(\alpha)} (\mathbf{m}^{(\alpha)} \otimes \mathbf{n}^{(\alpha)}) \tag{2}$$

Slip rate is determined according to the power law,

$$\dot{\gamma}^{(\alpha)} = \dot{\gamma}_0 \left| \frac{\tau^{(\alpha)}}{g^{(\alpha)}} \right|^n \operatorname{sign}(\tau^{(\alpha)}) \tag{3}$$

where $\tau^{(\alpha)}$ and $g^{(\alpha)}$ denote the resolved shear stress and slip resistance, respectively. Moreover, $\dot{\gamma}_0$ and n represent the reference slip rate and the rate sensitivity exponent. The slip resistance evolves according to

$$\dot{g}^{(\alpha)} = \sum_{\beta} h^{\alpha\beta} \left| \dot{\gamma}^{\beta} \right| \tag{4}$$

Peirce and Asaro's (sech) self-hardening law is utilized for the hardening,

$$h^{\alpha\alpha} = h(\gamma) = h_0 \operatorname{sech}^2 \left| \frac{h_0 \gamma}{g_s - g_0} \right| \tag{5}$$

where h_0 is the initial hardening modulus, g_0 is the initial slip resistance and g_s is the saturation slip resistance.

$$h^{\alpha\beta} = q^{\alpha\beta} h^{\alpha\alpha} \quad , \quad (\alpha \neq \beta) \tag{6}$$

Latent hardening moduli $h^{\alpha\beta}$ is calculated with constant q, the ratio of latent hardening to the self-hardening. All 12 slip systems of the FCC are taken as active slip systems.

3. Numerical Analysis

Crystal plasticity finite element framework is used for the numerical analysis. All the simulations are performed with the commercial finite element analysis software ABAQUS. A user-subroutine code (UMAT) is modified and used to define the mechanical behaviour of the polycrystal (see Huang (1991)). The material used in the study is aluminum AA6016 in T4 temper condition. The experimental data for the aluminum AA6016 in sheet form is taken from Granum et al. (2019) and used to calculate model parameters through a representative volume element (RVE) analysis with 300 grains. All the RVEs are created through polycrystal generation and meshing software Neper utilizing Voronoi tessellations (see Quey et al. (2011)). The symmetric boundary conditions are imposed for both the parameter identification and the main part. The strain rate is taken as 10^{-3} throughout the study.

Cubic elastic parameters for the aluminum sheet are used as $C_{11} = 108.2$ GPa, $C_{12} = 61.3$ GPa and $C_{44} = 28.5$ GPa (see e.g. Nakamachi et al. (2002)). The reference slip rate $\dot{\gamma}_0$ is taken as 10^{-3} and rate sensitivity exponent n is determined as 60. The ratio of latent hardening to the self-hardening q is taken as 1.4 due to the material investigated. Through the parameter identification procedure, hardening parameters are obtained as; initial hardening modulus $h_0 = 190$ MPa, saturation slip resistance $g_s = 95$ MPa and initial slip resistance $g_0 = 47$ MPa. This parameter set gives the closest stress response to the experimental data as shown in Fig. 1. To verify the obtained hardening parameters, three simulations are conducted with different sets of random orientation and all three resulted in almost identical curves, confirming the macroscopic isotropic response.

To represent different morphologies, different representative volume elements (RVEs) are generated with 300 grains. The average aspect ratio of the grains is adjusted such that the first RVE has equiaxed grains, while other RVEs have grains in the shape of needles. Needle RVEs have the ratio of longer dimension to the shorter dimension from 2 to 10, separately. Equiaxed, needle1, needle2 and needle3 RVEs are shown in Fig. 2. These morphologies

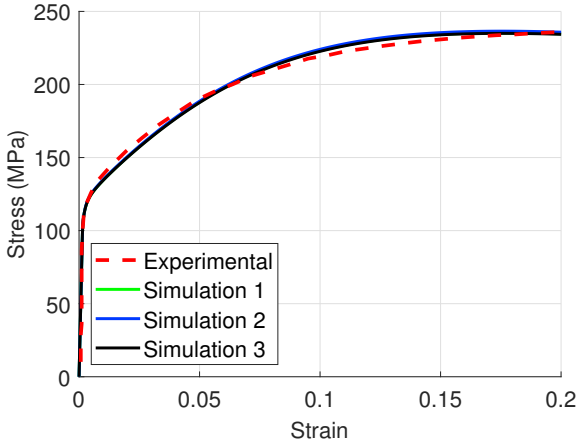

Fig. 1: Experimental versus RVE stress strain response under axial loading condition for three different randomly oriented grain microstructures.

consist of grains with mean aspect ratios of (1,1,1), (0.5,1,0.5), (0.25,1,0.25) and (0.1,1,0.1), respectively where the ratio of longer dimension to the shorter dimension is gradually increased.

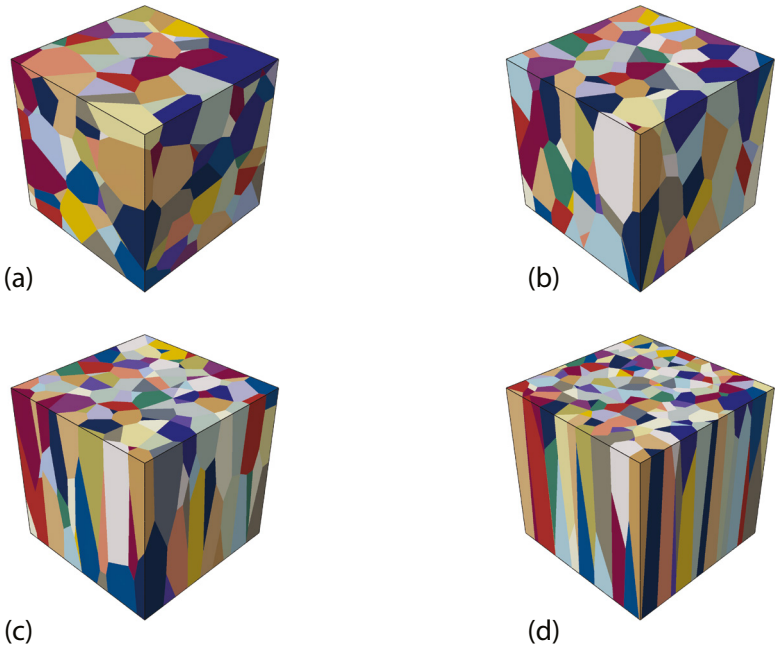

Fig. 2: RVEs with different grain morphology; (a) Equiaxed, (b) Needle1, (c) Needle2, (d) Needle3

RVE represents the smallest volume element that general behavior and the mean properties of the material can be observed. So, the boundary conditions must be adjusted such that RVE can imitate the mechanical response of the material. Symmetric boundary conditions are imposed such that all surfaces of RVEs are kept straight (see e.g. Yalçinkaya et al. (2019)). Also, given boundary conditions maintaned the triaxiality value at 0.33 (see e.g. Yalçinkaya et al. (2021a)). % 10 displacement is given to RVEs as the loading condition. After RVE analyses are completed, a post-process procedure with volumetric average (i.e. homogenization) is applied to find the stress-strain responses (see e.g. Tekoğlu (2014)).

3.1. Crystal orientations

For the orientation of the grains, Euler ZYX convention is implemented. From the local coordinate system to the global coordinate system, crystals of each grain are assigned to have a set of Euler rotations. In the case of the RVEs with randomly oriented grains, each grain has a unique set of Euler angles in the range of [0 360] for X and Z rotation and [0 180] for Y rotation. This set of angles provides the required randomness in terms of crystal orientation. Therefore, the isotropic macro response can be achieved with random Euler angles. Note that the local plasticity model used in the current study does not account for the effect of the grain boundaries through a specific model. Nevertheless, the crystal orientations are assigned randomly, so, there are orientation differences between adjacent grains which create such an effect that grains restrain each other from slip and rotation as if the model includes the grain boundaries.

For the RVEs with orientation alignment, grain orientations are distributed randomly within restricted intervals. Crystals are tilted around the building direction by imposing X and Z rotations while the Y rotation is always kept at zero. For instance, being oriented up to 10 degrees means an Euler transformation between local coordinates to global coordinates in such a way that the X and Z rotations are restricted to the interval of [-10 +10]. The rotation angles are selected randomly within their restricted intervals. The aim is to provide an orientation alignment to the material around the building direction while preserving the polycrystalline characteristic.

4. Results

Initially, the influence of the grain shape is addressed without considering the texture effect. In order to analyze solely the effect of the grain morphology the orientations in all RVEs with different aspect ratios are assigned randomly. The CPFE simulations are conducted by imposing % 10 displacement both in the building direction and the normal direction separately.

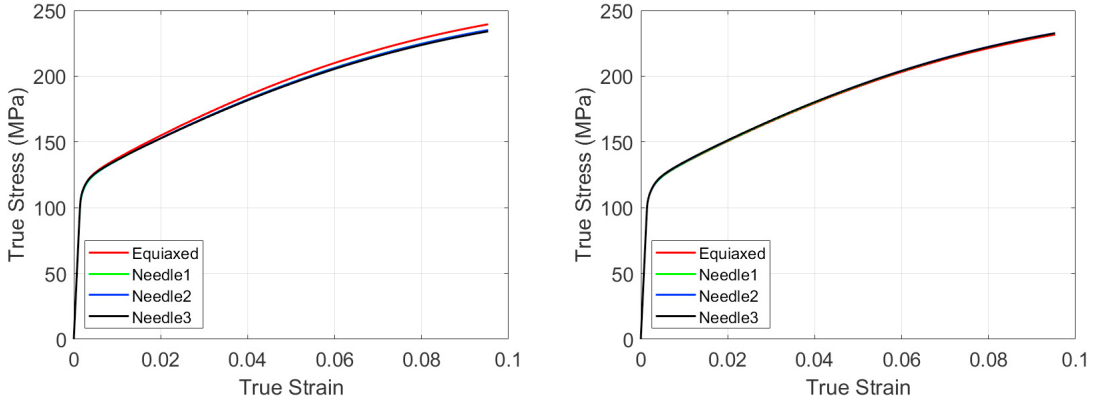

(a) Building direction loading (b) Normal direction loading

Fig. 3: Stress versus strain response for different microstructures with random orientations loaded in building and normal directions.

For both building and normal direction loading, the difference between constitutive response of RVEs is found to be negligible, as shown in Fig. 3. Although the grains are elongated gradually and reach a very columnar grain structure in needle3 case, the stress curves of the needle RVEs are very similar to that of equiaxed RVE. Even though the morphology has changed a lot, the crystal orientation of each grain is kept fully random in all RVEs in this simulation set. Considering the local plasticity model employed, the morphology itself did not make a significant difference. Morphologic differences without corresponding crystal orientation alignment are proven to be not much influential in the current numerical analysis. The possible usage of a strain gradient crystal plasticity model (see e.g. Yalçinkaya (2019), Yalçinkaya et al. (2021b), Yalçinkaya et al. (2021c)) would be quite problematic in this case due to the change in the mean grain size. Such a change would give non-physical results with considerable hardening.

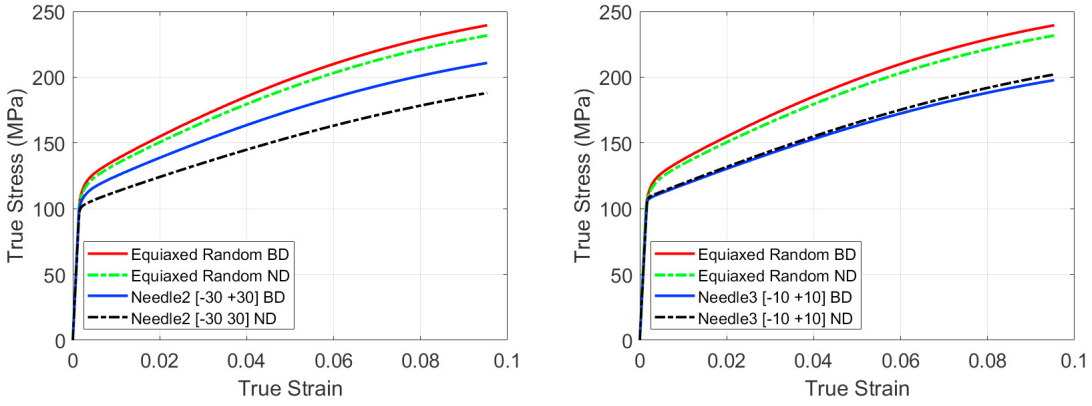

(a) Comparison of equiaxed and needle2

(b) Comparison of equiaxed and needle3

Fig. 4: Stress versus strain response for different microstructures loaded in building (BD) and normal direction (ND).

To have more realistic microstructures, the crystal orientations are assumed to be evolved with the elongation of the grains, i.e. aligned in the building direction. For the reference state unrestricted, fully random, orientations are assigned to the RVE with equiaxed grains. Then, the orientations are gradually restricted in narrower intervals as grains are more elongated along the building direction. Both X and Z rotations are restricted in [-90 +90], [-30 +30] and [-10 +10] intervals for RVEs called needle1 needle2 and needle3, respectively.

Fig. 4 demonstrates the stress versus strain response of RVEs having equiaxed and needle grains with corresponding orientation alignments. The first observation is that RVEs with elongated and textured grains possess weaker stress response compared to the RVE with randomly oriented equiaxed grains. For the textured RVEs, when the interval of orientation is kept in a narrower range, the orientations of individual grains become closer to each other. Since grains are oriented similarly, the indirectly imposed effect of the grain boundaries (misorientation) becomes more difficult to observe, especially for needle3. Since the the influence of the grain boundaries is still valid for the RVEs with the randomly oriented grains, they show higher resistance to the plastic deformation. Also, as illustrated in Fig. 4a, needle2 shows different responses for loadings in building and normal directions. Having grain orientations restricted in [-30 +30] interval, needle2 presents an anisotropic behaviour. On the other hand, randomly oriented RVE shows similar responses in both directions due to its isotropic structure. Likewise, as shown in Fig. 4b, strongly oriented needle3 also possesses similar responses for building and normal directions, but the reason for that is the crystal symmetry since the rotation angles are very small.

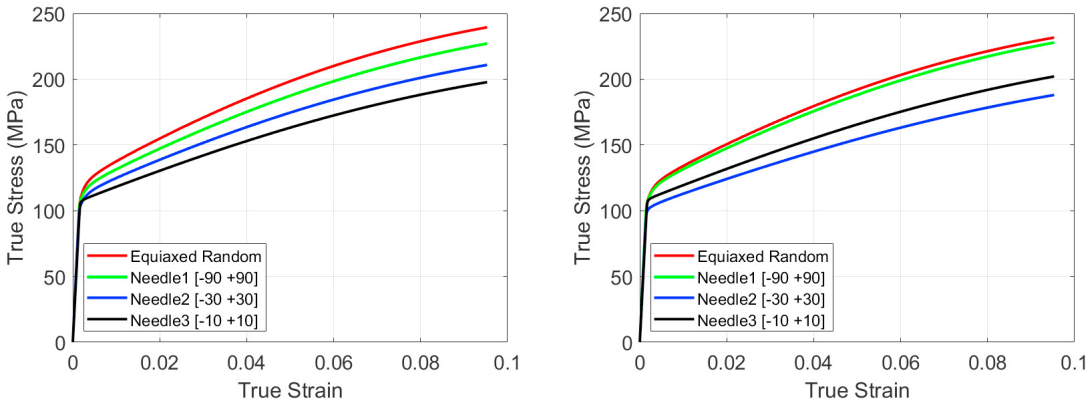

(a) Building direction loading

(b) Normal direction loading

Fig. 5: Stress versus strain response for microstructures with different morphologies and orientation alignment.

Stress-strain response curves of all RVEs are illustrated in Fig. 5 for loading along the building and the normal directions, separately. For both cases, the strongest response is obtained for the RVE with randomly oriented equiaxed

grains. As the grains are more elongated and crystal orientations are further restricted, the stress response is decreased. For the normal direction loading, the stress response of needle2 is lower than the response of needle3, due to the plastic anisotropy observed in needle2, as discussed earlier.

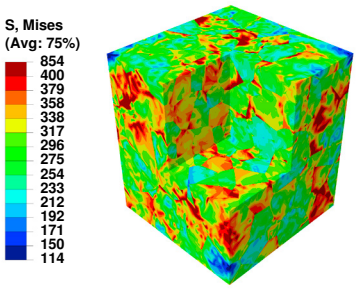

(a) Von Mises stress distribution of equiaxed RVE

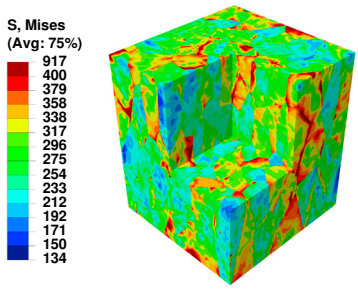

(b) Von Mises stress distribution of needle1 RVE

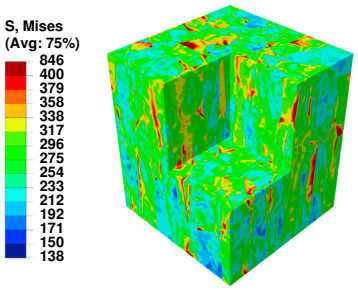

(c) Von Mises stress distribution of needle2 RVE

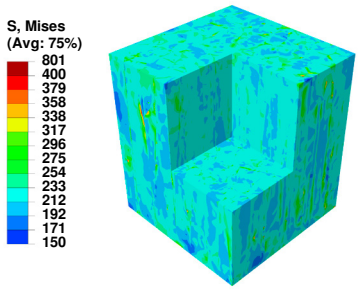

(d) Von Mises stress distribution of needle3 RVE

Fig. 6: Von Mises stress distribution for different microstructures loaded in the building direction.

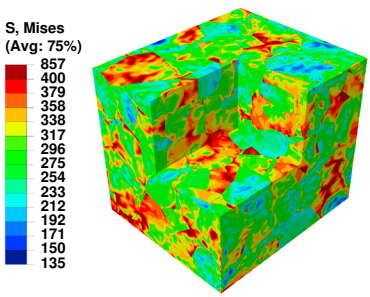

(a) Von Mises stress distribution of equiaxed RVE

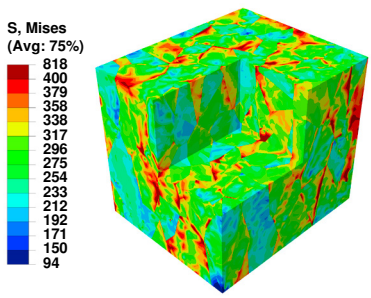

(b) Von Mises stress distribution of needle1 RVE

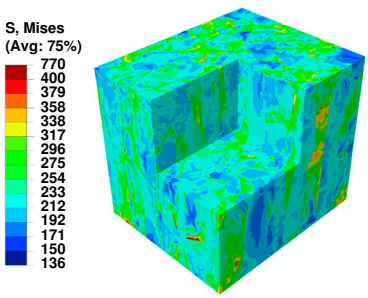

(c) Von Mises stress distribution of needle2 RVE

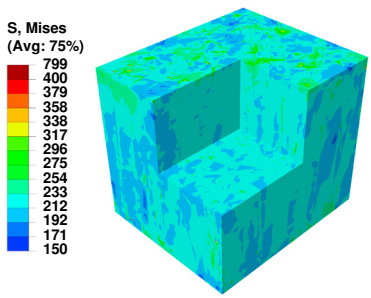

(d) Von Mises stress distribution of needle3 RVE

Fig. 7: Von Mises stress distribution for different microstructures loaded in the normal direction.

Von Mises equivalent stress contours for building and normal direction loadings are shown in Figs. 6 and 7 respectively. The lower stress response for RVEs with elongated and oriented grains can also be observed in von Mises stress distributions. Moreover, as the orientation alignment is increased, due to the diminishing of the misorientations between neighboring grains, more homogeneous stress distribution is observed in Figs. 6d and 7d.

5. Conclusions

In this paper, the mechanical behavior of the microstructures with columnar grains which are observed in additively manufactured metallic products is investigated through a crystal plasticity framework. Columnar grain structure and the corresponding orientation alignment are numerically modeled to assess the constitutive response and the anisotropy due to additive manufacturing. Step by step, the grains are elongated and the orientations are restricted around the building direction to analyze the anisotropy at different levels.

Firstly, the sole effect of morphology is studied by modeling the RVEs with different degree of columnar structure having randomly oriented grains, however the difference between the constitutive responses is found to be negligible. After assigning the corresponding restricted orientations to the morphologies, a significant difference occurs between flow stresses of RVEs with equiaxed and columnar grains for both building and normal direction loading. The stress response weakens as grains become more columnar. RVEs with grains oriented around the building direction demonstrates that when the orientation of each grain is assigned in a similar direction, the misorientation of the neighboring grains diminishes. Since the misorientations indirectly impose the effect of the grain boundaries, oriented RVE shows lower resistance to plastic deformation. The numerical results agree qualitatively with the literature. Final crystalline structure of additively manufactured products have significant importance in terms of mechanical properties.

References

Charmi, A., Falkenberg, R., Àvila, L., Mohr, G., Sommer, K., Ulbricht, A., Sprengel, M., Neumann, R., Skrotzki, B., Evans, A., 2021. Mechanical anisotropy of additively manufactured stainless steel 316L: An experimental and numerical study. Materials Science and Engineering: A 799, 140154.

Dumoulin, S., Engler, O., Hopperstad, O., S., Lademo, O., G., 2012. Description of plastic anisotropy in AA6063-T6 using the crystal plasticity finite element method. Modelling and Simulation in Materials Science and Engineering 20, 055008.

Frazier, W., 2014. Metal Additive Manufacturing: A Review. Journal of Materials Engineering and Performance 23, 1917–1928.

Ghorbanpour, S., Alam, M., E., Ferreri, N., C., Kumar, A., McWilliams, B., A., Vogel, S., C., Bicknell, J., Beyerlein, I., J., Knezevic, M., 2020. Experimental characterization and crystal plasticity modeling of anisotropy, tension-compression asymmetry, and texture evolution of additively manufactured Inconel 718 at room and elevated temperatures. International Journal of Plasticity 125, 63–79.

Granum, H., Aune, V., Børvik, T., Hopperstad, O., S., 2019. Effect of heat-treatment on the structural response of blast-loaded aluminium plates with pre-cut slits. International Journal of Impact Engineering 132, 103306.

Guden, M., Yavaş, H., Tanrikulu, A., A., Tasdemirci, A., Akın, B., Enser, S., Karakuş, A., Hamat, B., A., 2021. Orientation dependent tensile properties of a selective-laser-melt 316L stainless steel. Materials Science and Engineering: A 824, 141808.

Hovig, E., Azar, A., Grytten, F., Sørby, K., Andreassen, E., 2018. Determination of Anisotropic Mechanical Properties for Materials Processed by Laser Powder Bed Fusion. Advances in Materials Science and Engineering 2018, 1–20.

Huang, Y., 1991. A user-material subroutine incroporating single crystal plasticity in the abaqus finite element program. Mech Report 178.

Ishimoto, T., Hagihara, K., Hisamoto, K., Nakano, T., 2021. Stability of crystallographic texture in laser powder bed fusion: Understanding the competition of crystal growth using a single crystalline seed. Additive Manufacturing 43, 102004.

Ishimoto, T., Hagihara, K., Hisamoto, K., Sun, S., H., Nakano, T., 2017. Crystallographic texture control of beta-type Ti–15Mo–5Zr–3Al alloy by selective laser melting for the development of novel implants with a biocompatible low Young's modulus. Scripta Materialia 132, 34–38.

Karakaş, A., Fenercioğlu, T.O., Yalçinkaya, T., 2021. The influence of flow forming on the precipitation characteristics of Al2024 alloys. Materials Letters 299, 130066.

Kergaßner, A., Mergheim, J., Steinmann, P., 2019. Modeling of additively manufactured materials using gradient-enhanced crystal plasticity. Computers & Mathematics with Applications 78, 2338–2350.

Kok, Y., Tan, X., P., Wang, P., Nai, M., L., Loh, N., H., Liu, E., Tor, S., B., 2018. Anisotropy and heterogeneity of microstructure and mechanical properties in metal additive manufacturing: A critical review. Materials & Design 139, 565–586.

Lopes, A., Barlat, F., Gracio, J., Duarte, J., Rauch, E., 2003. Effect of texture and microstructure on strain hardening anisotropy for aluminum deformed in uniaxial tension and simple shear. International Journal of Plasticity 19, 1–22.

Moussaoui, K., Rubio, W., Mousseigne, M., Sultan, T., Rezai, F., 2018. Effects of Selective Laser Melting additive manufacturing parameters of Inconel 718 on porosity, microstructure and mechanical properties. Materials Science and Engineering: A 735, 182–190.

Nakamachi, E., Xie, C., Morimoto, H., Morita, K., Yokoyama, N., 2002. Formability assessment of FCC aluminum alloy sheet by using elastic/crystalline viscoplastic finite element analysis. International Journal of Plasticity 18, 617–632.

Qiu, C., Adkins, N., Attallah, M., 2013. Microstructure and tensile properties of selectively laser-melted and of HIPed laser-melted Ti-6Al-4V. Materials Science and Engineering: A 578, 230–239.

Quey, R., Dawson, P., Barbe, F., 2011. Large-scale 3D random polycrystals for the finite element method: Generation, meshing and remeshing. Computer Methods in Applied Mechanics and Engineering 200, 1729–1745.

Song, B., Zhao, X., Li, S., Han, C., Wei, Q., Wen, S., Liu, J., Shi, Y., 2015. Differences in microstructure and properties between selective laser melting and traditional manufacturing for fabrication of metal parts: A review. Frontiers of Mechanical Engineering 10, 111–125.

Tekoğlu, C., 2014. Representative volume element calculations under constant stress triaxiality, Lode parameter, and shear ratio. International Journal of Solids and Structures 51, 4544–4553.

Thijs, L., Verhaeghe, F., Craeghs, T., Humbeeck, J., Kruth, J., P., 2010. A study of the microstructural evolution during selective laser melting of Ti–6Al–4V. Acta Materialia 58, 3303–3312.

Wang, Z., Guan, K., Gao, M., Li, X., Chen, X., Zeng, X., 2012. The microstructure and mechanical properties of deposited-IN718 by selective laser melting. Journal of Alloys and Compounds 513, 518–523.

Yalçinkaya, T., 2019. Strain gradient crystal plasticity: Thermodynamics and implementation. Handbook of Nonlocal Continuum Mechanics for Materials and Structures , 1001–1033.

Yalçinkaya, T., Çakmak, S.O., Tekoğlu, C., 2021a. A crystal plasticity based finite element framework for RVE calculations of two-phase materials: Void nucleation in dual-phase steels. Finite Elements in Analysis and Design 187, 103510.

Yalçinkaya, T., Gungor, G., Çakmak, S.O., Tekoğlu, C., 2019. A Micromechanics Based Numerical Investigation of Dual Phase Steels. Procedia Structural Integrity 21, 61–72.

Yalçinkaya, T., Özdemir, İ., Tandoğan, İ., T., 2021b. Misorientation and grain boundary orientation dependent grain boundary response in polycrystalline plasticity. Computational Mechanics 67, 937–954.

Yalçinkaya, T., Tandoğan, İ., T., Özdemir, İ., 2021c. Void growth based inter-granular ductile fracture in strain gradient polycrystalline plasticity. International Journal of Plasticity 147, 103123.

Yalcinkaya, T., Brekelmans, W.A.M., Geers, M.G.D., 2008. BCC single crystal plasticity modeling and its experimental identification. Modelling and Simulation in Materials Science and Engineering 16, 085007.

Yasa, E., Deckers, J., Kruth, J., P., 2011. The investigation of the influence of laser re-melting on density, surface quality and microstructure of selective laser melting parts. Rapid Prototyping Journal 17, 312–327.

Zhang, B., Liu, S., Shin, Y., 2019. In-Process monitoring of porosity during laser additive manufacturing process. Additive Manufacturing 28, 497–505.

Zhang, K., Holmedal, B., Hopperstad, O., S., Dumoulin, S., Gawad, J., Van Bael, A., Van Houtte, P., 2015. Multi-level Modelling of Mechanical Anisotropy of Commercial Pure Aluminium Plate: Crystal Plasticity Models, Advanced Yield Functions and Parameter Identification. International Journal of Plasticity 66, 3–30.

Zhao, Q., Wahab, M., Ling, Y., Liu, Z., 2021. Grain-orientation induced stress formation in AA2024 monocrystal and bicrystal using Crystal Plasticity Finite Element Method. Materials & Design 206, 109794.

Zhou, X., Li, K., Zhang, D., Liu, X., Ma, J., Liu, W., Shen, Z., 2015. Textures formed in a CoCrMo alloy by selective laser melting. Journal of Alloys and Compounds 631, 153–164.